MICROROBOTS

MiGriBot: A miniature parallel robot with integrated gripping for high-throughput micromanipulation

Maxence Leveziel, Wissem Haouas, Guillaume J. Laurent, Michaël Gauthier, Redwan Dahmouche*

Although robotic micromanipulation using microtweezers has been widely explored, the current manipulation throughput hardly exceeds one operation per second. Increasing the manipulation throughput is thus a key factor for the emergence of robotized microassembly industries. This article presents MiGriBot (Millimeter Gripper Robot), a miniaturized parallel robot with a configurable platform and soft joints, designed to perform pick-and-place operations at the microscale. MiGriBot combines in a single robot the benefits of a parallel kinematic architecture with a configurable platform and the use of soft joints at the millimeter scale. The configurable platform of the robot provides an internal degree of freedom that can be used to actuate microtweezers using piezoelectric bending actuators located at the base of the robot, which notably reduces the robot's inertia. The soft joints make it possible to miniaturize the mechanism and to avoid friction. These benefits enable MiGriBot to reach a throughput of 10 pick-and-place cycles per second of micrometer-sized objects, with a precision of 1 micrometer.

INTRODUCTION

Increasing the throughput of robotic manipulators to reduce production costs and to improve the volume of production has been a challenge for decades. The need is even greater at small scales, where the level of production [such as MEMS (microelectromechanical systems) and microelectronics] is huge. Recent works in microrobotics have paved the way to the development of miniaturized parallel manipulators, whose low moving mass makes it possible to reach unequaled speeds for contact-based micromanipulation. One of the groundbreaking results is the milliDelta (*1*), which is a Delta-like miniaturized parallel robot able to perform in high-speed trajectories, such as circles, with a frequency up to 75 Hz. Parallel kinematic architectures (*2*) have several benefits compared with serial architectures. First, the actuators can be fixed on the robot's base, leading to lighter moving parts. In addition, the moving platform is more rigid than its serial counterpart for an equivalent moving mass. The combination of the high rigidity and light moving parts increases the natural frequencies of the robot's structure and allows high-speed positioning. One of the most common parallel architectures that illustrate these benefits is the Delta robot (*3*, *4*), which has three translational degrees of freedom (DoFs). Its high speed makes it particularly suitable when high-throughput pick-and-place operations are required, such as in the electronics industry (*5*).

Another advantage of parallel robot structures is that they can generate controlled rotations from linear actuators. The combination of microtransducers that are able to generate high-speed translation, such as piezo-stacks and piezo-benders (*6*, *7*), with lightweight parallel structures can permit several DoFs and achieve short response times. However, because classical spherical, universal, and revolute joints cannot be miniaturized under a certain level, they are replaced by flexure hinges. The resulting benefit is that, contrary to classical mechanisms, compliant structures do not introduce backlash and friction in the mechanical system. Submicrometer precision can thus be achieved using this class of structures (*8*, *9*). However, compliant joints are usually obtained through notch hinges and leaf-spring hinges that have small deformation amplitudes, which considerably limit the workspace of this type of robot (*10*–*12*).

A possible way to enlarge the workspace is to make the links wholly deformable, which leads to parallel continuum robots (*13*–*15*). However, the development of accurate models for these classes of robots is complex, and their inversion is time-consuming, leading to low-frequency control loops (*16*–*19*). Another solution is to use a combination of hard and soft materials to obtain the desired soft-joint behavior. For revolute joints, the preferred technique is to laminate a rigid layer for the rigid links with a flexible layer for the hinges (*20*). The lamination is regularly performed with carbon-fiber sheets as rigid links and polyimide films for the flexible joints. The milliDelta and many miniature robots rely on this technique, using diverse materials (*1*, *21*–*23*). Spherical joints can be obtained using elastomeric parts between rigid links (*24*, *25*). These soft joints can be produced through photolithography (*26*, *27*) or by molding in silicon microstructures (*28*).

However, the predominant issue with current parallel miniaturized robots is their lack of grasping ability (*29*, *30*). The addition of a microgripper on top of a miniaturized moving platform markedly increases the moving mass, decreases the dynamic performances, and requires electrical connections through the robot structure, which is particularly difficult to integrate at small scales. Instead, current miniaturized robots are designed as positioning tables that can be used in combination with an independent motionless gripper.

Parallel architectures with a configurable platform provide a solution to the limited grasping and manipulation functions of robots without the need for an additional gripper. The kinematics of this class of robots offers additional DoFs to the mobile platform that are actuated from the base through the robots' links (*31*, *32*). These DoFs are thus part of the kinematic architecture of the robots and do not require actuators on the platform. The additional DoF of the configurable platform can be used to generate additional mobility, such as a rotational motion (*33*, *34*) or grasping (*35*, *36*). In this field, several parallel structures allowing up to eight DoFs (three translations + three rotations + grasping + in-hand rotation) have been recently proposed (*37*). The four-DoF Quattro Robot from OMRON-ADEPT (*38*) also belongs to this class of robots. It reaches

FEMTO-ST Institute, CNRS, Univ. Bourgogne Franche-Comté, 24 rue Alain Savary, F-25000 Besançon, France.
*Corresponding author. Email: redwan.dahmouche@femto-st.fr

200 picks per minute for the standard industrial cycle of ADEPT's pick and place, which makes it one of the fastest industrial robots. However, these manipulators with integrated grasping are composed of classical spherical joints. Consequently, no miniaturized parallel robot based on soft joints and having a configurable platform has been proposed yet.

Here, we present MiGriBot (Millimeter Gripper Robot), a miniaturized parallel robot combining a configurable platform and soft joints (Fig. 1). The four-DoF kinematic architecture of MiGriBot allows it to grasp and manipulate micro-objects (three translations + grasping). The structure of MiGriBot is composed of a millimeter-scale parallel mechanism actuated with four piezoelectric actuators (movie S1). It permits 10 pick-and-place operations per second for the ADEPT's cycle of 200/600/200 μm (which stands for a 200-μm pick motion, followed by a 600-μm horizontal displacement, and a 200-μm place motion) due to its integrated grasping capability. The precision of MiGriBot is around 1 μm.

RESULTS

Robotic structure and design

The miniature robotic structure is composed of an actuation system and a parallel mechanism (Fig. 2, A and B). The actuation system consists of four multilayered piezoelectric bending actuators with embedded position sensors. Extensions were attached to the actuator's tips to amplify the output displacements. The stroke of each actuator with its extension was 1 mm (±0.5 mm). Two actuators move along the x axis and two along the y axis. Given the ratio between the length of the actuation system (54.5 mm) and the piezo-bender strokes, the movement of the extension tips can be considered translational. The parallel mechanism (fig. S1) is composed of silicon rigid links and polydimethylsiloxane (PDMS) soft joints that act as spherical joints in the structure (Fig. 2C). A pair of same PDMS joints was used to allow the platform to fold. This additional DoF was used to grasp micro-objects due to the tweezers mounted on the configurable platform. The configurable platform can be folded with coordinated movement of the four limbs (Fig. 2D). Thus, the four DoFs of the robot, three translational and one grasping, were controlled by the four piezo-benders located on the robot's base (movie S2). Because no additional active gripper is required, the robot structure is lighter. In addition, no wires (power, signals) were attached to the robot platform, which eliminated unnecessary disturbances from the configurable platform.

MiGriBot is compact compared with common solutions. The tweezers and its actuators are attached to the rigid platform of a parallel structure. The overall dimensions of the parallel mechanism are 22 mm by 19 mm by 0.4 mm. The fabrication of the compliant mechanism consisted of molding soft joints into a silicon structure made with cleanroom microfabrication techniques (see Materials and Methods). To prevent the separation of the soft joints from the links, we used a specific shape inspired by the design proposed by Vogtmann *et al.* (*24*) as shown in Fig. 3F. The robot was thus made in the planar configuration. Next, the tweezer's arms were assembled on the platform (Fig. 3A). Subsequently, the base of each limb was glued onto the actuators' extensions (Fig. 3B). The parallel mechanism was then folded from its initial planar configuration (Fig. 3C) to reach the "home configuration" (Fig. 3D), which corresponded to the center of the stroke of the actuators (*39*).

Finite element analysis (FEA) performed on the whole parallel mechanism using Ansys showed that the joints should not experience any damage in the full range of actuation (Fig. 3, D and E). In addition, the FEA allowed us to predict the parallel mechanism behavior from the planar configuration (obtained at the end of the fabrication process) to any pose of the micromanipulator. The FEA showed that the deformation of the soft joint was similar to a rotation around the center of the PDMS part, acting as pseudo-spherical joints.

Robotic micromanipulator performance

This section presents the robot's performances in terms of workspace, precision, and pick-and-place cycles. The elevation of the home configuration of the manipulator was chosen to maximize the accessible workspace and to avoid singularities, positions in which we might lose control of at least one DoF (*39*).

The mechanism has at least two singular positions: the planar configuration and the configuration in which the links are perpendicular to the platform. The workspace corresponding to the chosen elevation was computed and is illustrated in Fig. 4 (A and B). The home configuration was defined by the actuators being in the middle of their stroke. The elevation of the home configuration could

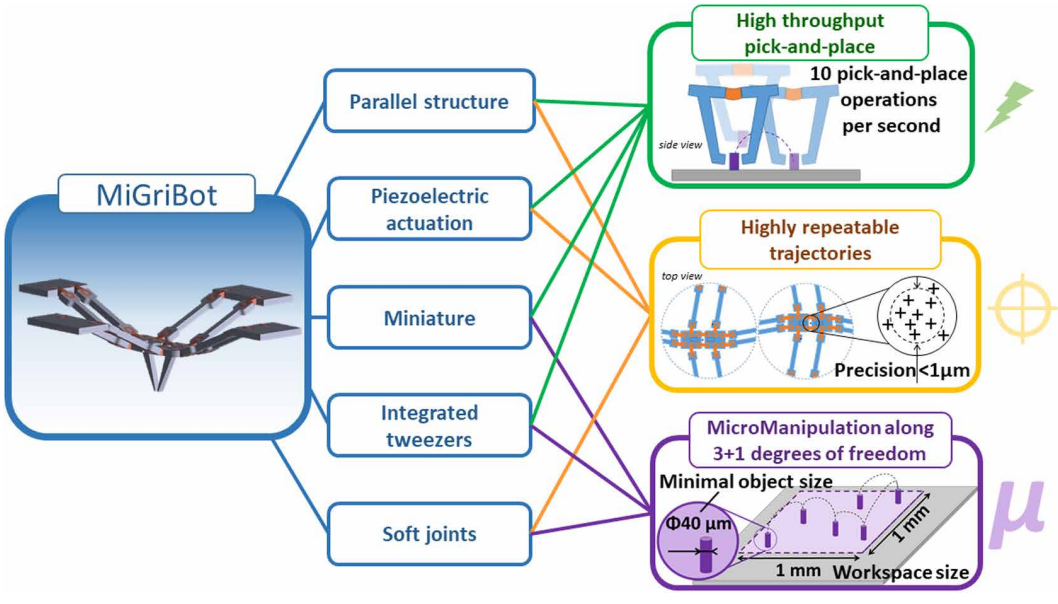

Fig. 1. Characteristics of MiGriBot. MiGriBot is a miniature robotic manipulator combining a configurable platform and soft joints that performs in high-throughput trajectories and the picking and placing of micro-objects along a relatively large workspace.

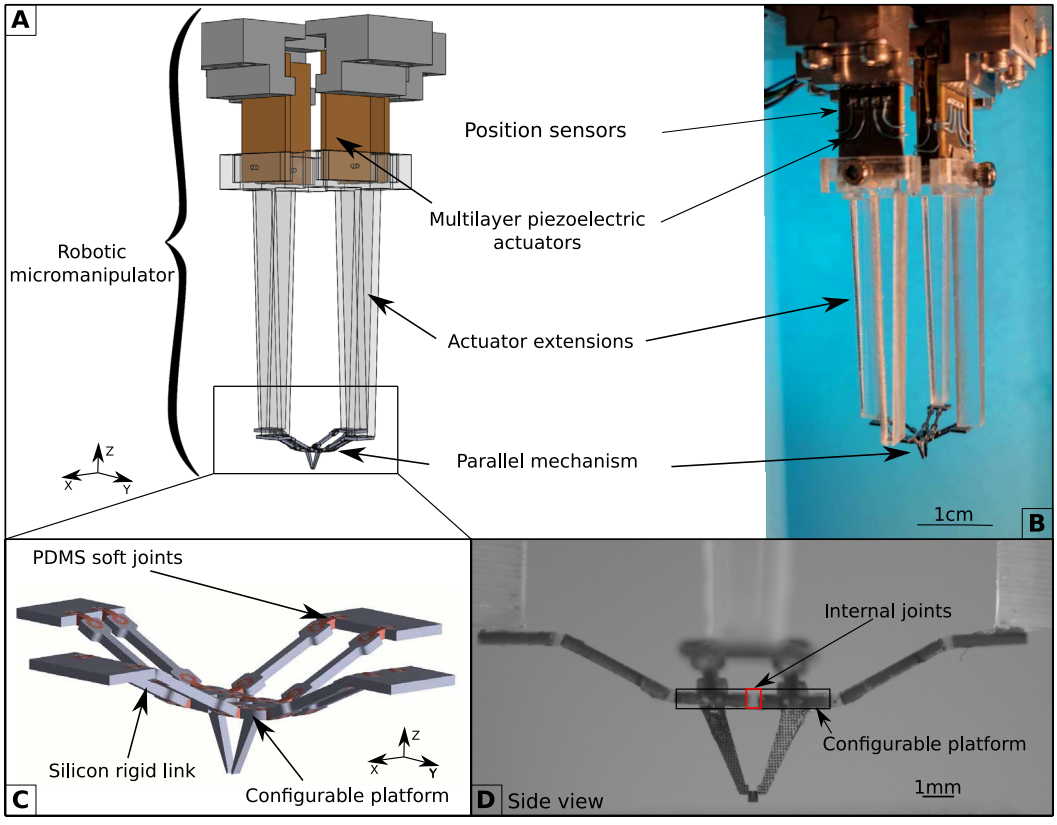

Fig. 2. Design of the robotic micromanipulator. (**A**) Design of the robotic micromanipulator with the actuation system (composed of four multilayered piezoelectric actuators with extensions to amplify their displacements) and the parallel mechanism. (**B**) Picture of the experimental robotic micromanipulator composed of the actuation system and the parallel mechanism. (**C**) Close-up of the parallel mechanism composed of silicon rigid links, soft PDMS joints, and a configurable platform with two internal soft joints. (**D**) Side view of the experimental parallel mechanism grasping a cylinder with a diameter of 350 μm and a height of 400 μm.

be adjusted by setting the distances between the actuators. Given the dimensions of the manipulator, the workspace was maximized when the elevation of the home configuration corresponded to $z_{home} = -2.35$ mm (Fig. 3D) and when the horizontal position was $x_{home} = y_{home} = 0$ in the reference frame R_0.

Workspace of the micromanipulator

The horizontal workspace (parallel to the *OXY* plane) was maximized at the elevation of the home configuration. From this configuration, the entire actuator stroke was used to move the platform in the horizontal plane, and the workspace was consequently a square whose side was the actuator stroke (Fig. 4B). The workspace was also analyzed regarding two particular cases: when the tweezers were fully closed and when the tweezers were fully opened. Because the tweezers' actuation was integrated within the structure, we observed that it had an influence on the workspace (Fig. 4A). The manipulation workspace was the intersection of both extreme cases, making it possible to fully open and close the tweezers everywhere in this workspace (green zone in Fig. 4A). However, because the top of the workspace (orange zone in Fig. 4A) was reachable with closed tweezers, it could be used during the manipulation to transfer the grasped objects without releasing them. Because of the structural symmetry of the robotic manipulator, the same workspace was obtained in the *OXZ* plane and *OYZ* plane.

Experimental measurements of the workspace were performed and showed good agreement with the model. Some characteristic points (the furthest-left, the furthest-right, the top, and the bottom positions of the manipulation workspace) are visible in Fig. 4 (C to F). The slight deviation between the experiments and theory visible at the top of the workspace (Fig. 4, A and F) was mainly due to uncertainties in the assembly process between the parallel mechanism and the actuation system inducing a small amount of asymmetry, which can be seen in Fig. 4F. The tweezer opening was also experimentally measured. Figure 4 (G and H) presents the closed and opened tweezers in the home configuration; the maximum size for the opening was 540 μm.

Positioning precision

Before mounting the robotic structure, we performed an evaluation of the precision of the actuation system in quasi-static. The measured precision, expressed as the standard deviation of the position after 30 repeated visits, was below 200 nm for positioning the tips of the actuator extensions.

After characterizing the quasi-static performances of the actuation system, we studied the precision of the whole robotic micromanipulator (fig. S2). Because of the symmetry of the structure, we measured the positioning precision only along two axes: the *z* axis and the *y* axis. In the case of the *y* axis, the structure had a low influence on the positioning, because we measured a precision of 600 nm. In the *z* axis, as the structure was deformed and the soft joints were more stressed, we observed a difference in terms of precision compared with the *x* and *y* axes. In this case, the obtained precision was around 1 μm (fig. S2).

Lifting capabilities

When manipulating an object, tweezers should apply a constant force. Because our robotic structure is overconstrained when the gripper is closed, the grasping forces will be distributed over the manipulator structure. Compliance in the manipulator is thus required to perform robotic pick-and-place operations. In our system, the stiffness of the compliant mechanism is actually lower than the stiffness of the actuator system, which can be considered rigid. The manipulator's compliance is consequently due to the soft joints. The FEA described in Fig. 3 made it possible to estimate this compliance for any configuration. For instance, the stiffness of the tweezers in the home configuration was 24.5 N m^{-1}, enabling a maximum

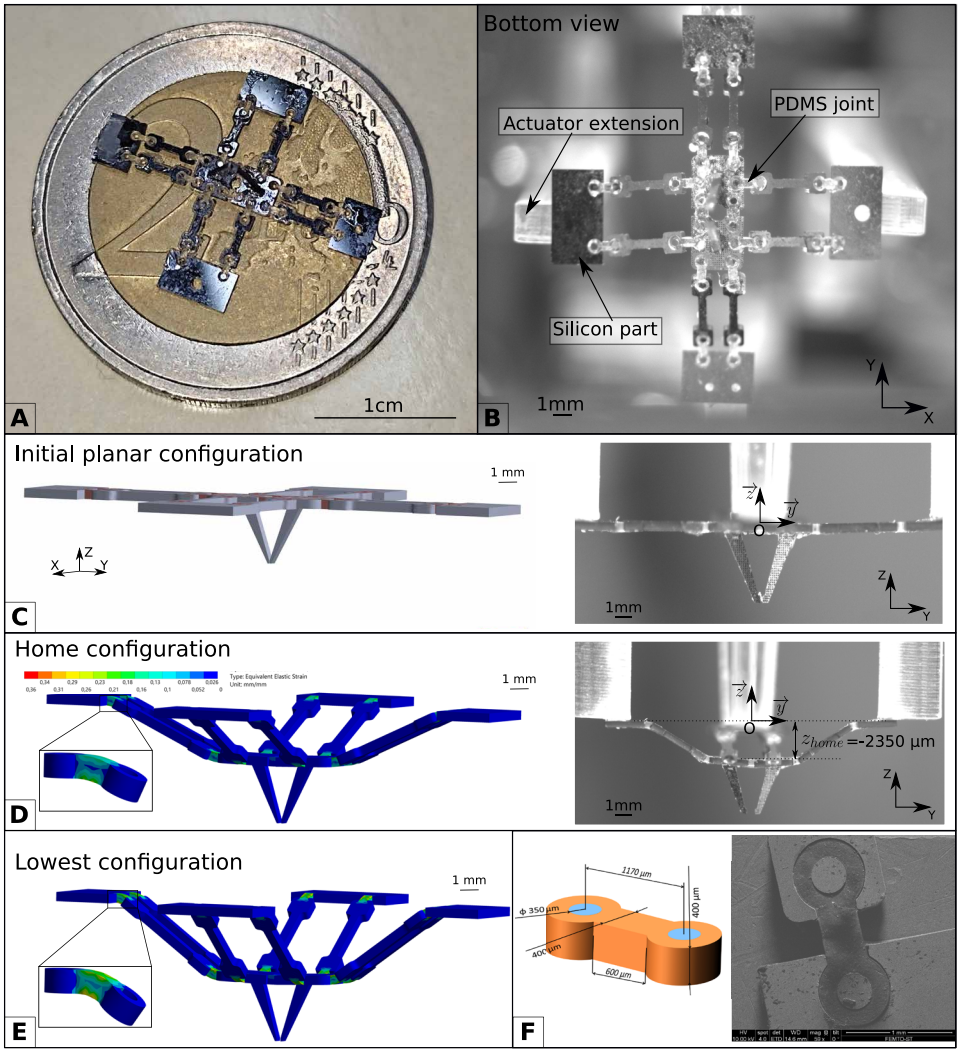

Fig. 3. Microfabrication and mechanical modeling of the parallel mechanism. (**A**) Parallel mechanism in planar configuration after the assembly of the tweezers. (**B**) Bottom view of the parallel mechanism attached to the actuation system. (**C**) Manipulator in the initial planar configuration at the end of the fabrication process (please note that the center O of our reference frame $R_0(O,\vec{x},\vec{y},\vec{z})$ is defined as the center of the top surface of the parallel mechanism in the initial planar configuration). (**D**) Mechanical model and experimental view of the manipulator in the home configuration and zoom on the mechanical constraint in a soft joint. (**E**) Mechanical model when the manipulator is in the lowest configuration. (**F**) Dimension of the PDMS soft joint (before deformation) and example of a scanning electron microscopy image of a soft joint.

grasping force of 6.6 mN, which was approximately 10 times larger than the parallel mechanism weight.

Given this theoretical grasping force, an experimental validation was performed to evaluate the lifting force. To obtain the maximum mass that the robot could move from one point to another, we conducted several tests with objects of increasing weight. The results showed that MiGriBot could manipulate objects with weights up to 80 mg but was not able to lift 110 mg (movie S7). The ratio between the theoretical grasping force and the highest weight the robot could lift (between 80 and 110 mg) corresponded to a friction coefficient between 0.11 and 0.16, which is a plausible friction coefficient range for a silicon/stainless-steel contact. Moreover, 80 mg is greater than the weight of the parallel mechanism (65 mg) and sufficiently high when compared with the size of the objects to be manipulated (for example, the mass of the cylinder used in the pick-and-place experiments is 0.07 mg).

High-throughput pick and place

The main function of MiGriBot is to manipulate micro-objects at high throughput. The dynamic performances of the micromanipulator and the actuation system were analyzed and experimentally characterized. Regarding the actuation system, the controllers were tuned to obtain a settling time below 10 ms without overshoot, and the resulting cutoff frequency was 110 Hz (fig. S6).

To avoid disturbances due to resonance, we designed the compliant mechanism to have an initial resonant frequency at least twice as high as the cutoff frequency of the actuators. The FEA provided the modal analysis of the compliant systems (movie S3 and table S1) and showed that the first resonance frequency was 264 Hz, in accordance with requirements.

To experimentally validate the capabilities of the designed robotic micromanipulator, we performed the pick-and-place of a silicon cylinder with a diameter of 350 µm and a height of 400 µm at low and high speeds. To facilitate comparisons, the pick-and-place cycle corresponded to a standard ADEPT cycle of 200/600/200 µm. It was composed of six steps: the closing of the tweezers to grasp the object from the initial position, the displacement to a target position, the opening of the tweezers to release the object, the second grasping, the displacement back to the initial position, and, last, the opening of the tweezers. The whole cycle is described experimentally in movie S4 with a decomposition of each part of the cycle. This cycle was tested on both low-speed manipulation and high-speed manipulation considering total cycle times of 2 s and 100 ms, respectively.

We demonstrated high-speed cycles of 100 ms (Fig. 5A). Although the slight dynamic effects visible in the high-speed cycle (Fig. 5B) induced small errors on the platform trajectory (Fig. 5C), the pick-and-place operations were successful in the high-speed cycle (movie S6). It showed that MiGriBot can achieve 10 pick-and-place cycles per second of micro-objects (including forward and backward movement).

A one-way pick-and-place cycle was also tested at high speed. This cycle involved five steps: the movement from the start position to the picking position, the closing of the tweezers to grasp the

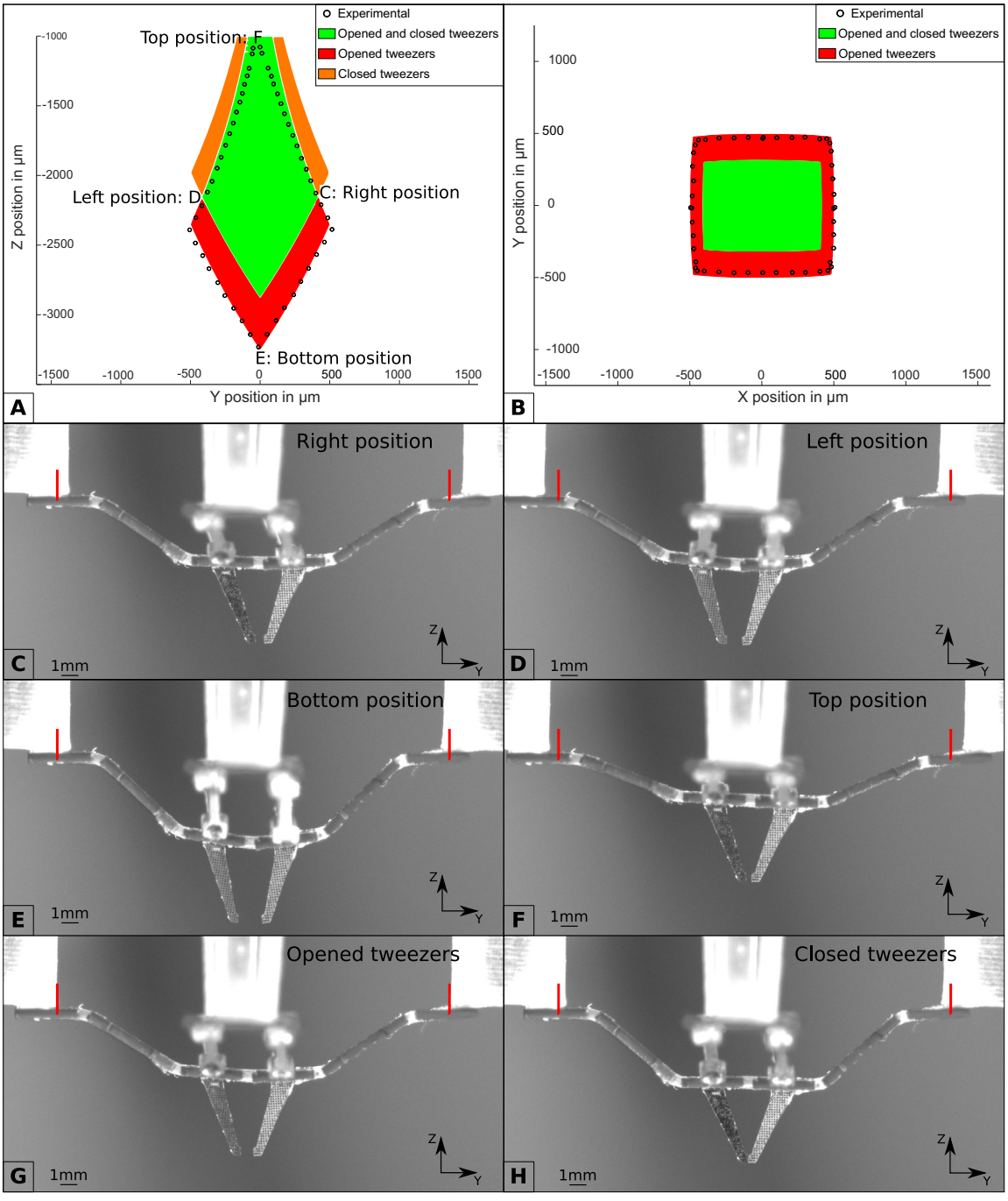

Fig. 4. Workspace of the micromanipulator. (**A**) Side view (*OYZ*) of the theoretical and experimental workspaces of the micromanipulator; in green, the workspace accessible whatever the state of the tweezers; in orange, the part accessible only with the closed tweezers; in red, the part accessible only with the opened tweezers. (**B**) Top view (*OXY*) of the theoretical and experimental workspaces of the micromanipulator. (**C**) Extreme-right position along *y* axis. (**D**) Extreme-left position along *y* axis. (**E**) Extreme-bottom position along *z* axis. (**F**) Extreme-top position along *z* axis. (**G**) Opened tweezers around home position. (**H**) Closed tweezers at home position.

object, the displacement to the target position, the opening of the tweezers to release the object, and the movement back to the start position. The distance between the picking place and the placing position was 600 µm. This one-way cycle was performed within 80 ms, which can be explained by the lack of need to open and close the gripper twice in comparison with the previous cycle. This cycle was successfully validated using three different objects with thicknesses of 40, 150, and 350 µm (movie S8).

To show the reproducibility in the handling of the objects by the micromanipulator, we performed 10 pick-and-place actions sequentially with the low-speed cycle (fig. S3 and movie S5). Given the cut-off frequency of the actuators and the first resonance frequency of

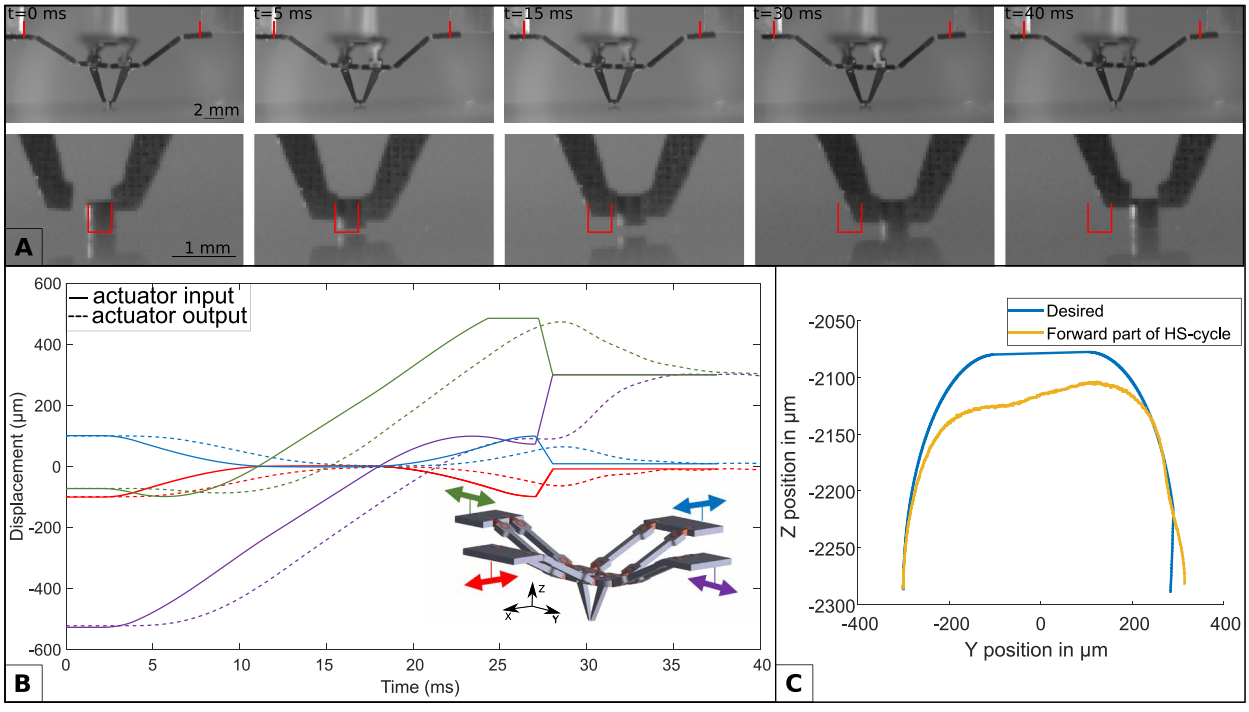

Fig. 5. Experimental demonstration of pick-and-place operations. The manipulated object is a 350-µm-diameter and 400-µm-height silicon cylinder, and the result is presented for the forward part of the high-speed cycle. (**A**) Motion capture of the manipulator for a pick-and-place high-speed cycle; initial positions of the actuators and the object are represented in red. (**B**) Command vector of each actuator versus the output vector during the forward part of a high-speed cycle. (**C**) Trajectory of the end-effectors in the (*OYZ*) plane for the reference cycle (blue) and high-speed (HS) cycle (yellow).

the robotic structure, the low-speed cycle was considered to be in a quasi-static mode.

Performance analyses

After validating that MiGriBot can successfully perform high-speed pick-and-place actions, we investigated its dynamic limits. To study this, we executed the displacement between the pick and the place locations of the described cycle at higher speeds without any load in the tweezers, and we compared the obtained trajectory with the reference trajectory. In the high-speed cycle, the forward trajectory, from the initial position to the target position, took 25 ms. Figure 6A presents the side view (in *OYZ*) of the experimental trajectories for different traveling times. As expected, we can see from this figure that the obtained trajectories became increasingly distant from the reference trajectory as the speed increased. It was also observed that the three trajectories (100, 25, and 15 ms) were in accordance with the reference. However, the 7-ms trajectory did not correspond to the reference trajectory, which indicated that the impact of inertia and the actuation system dynamic significantly increased between 15 and 7 ms.

To analyze the influence of the robot dynamics on a trajectory that involved more coupling between the several DoFs of the robot, we considered a 600-µm circular trajectory (Fig. 6, B and C). Considering 10 turns per second (10 Hz), the robotic manipulator was able to follow the reference trajectory. The radius of the circle decreased as the frequency increased. The −3-decibel cutoff frequency of the executed trajectory was approximately 50 Hz. Because the first resonance frequency of MiGriBot was as high as 264 Hz, the resonance mode was not reached. In the various experiments at high speed, no vibrations of the parallel mechanism were observed, which was consistent with the theoretical analysis.

To illustrate the versatility of MiGriBot, several objects were tested for grasping (Fig. 7). We demonstrated that the robotic micromanipulator was capable of grasping objects with widths between 40 and 400 µm. For instance, the robot handled watch ruby pieces with cylindrical and parallelepiped shapes (Fig. 7, A and B), and it successfully grasped a wire with a diameter of 40 µm (Fig. 7C) and inserted it into a 50-µm bore (movie S9). Larger objects were tested, such as watch gears (Fig. 7, D and E) and the parallel mechanism of another MiGriBot (Fig. 7F), which demonstrated that the manipulator was able to hold objects as heavy as its own parallel mechanism weight.

DISCUSSION

MiGriBot is a miniature robot able to manipulate objects as thin as 40 µm and to perform up to 10 pick-and-place operations per second (for ADEPT's cycle 200/600/200 µm). It is based on a parallel robotic architecture with soft joints and a configurable platform, which is used to ensure its grasping capability. All the DoFs of the robot, including grasping, are actuated from the robot's base using piezoelectric cantilever beams. The compliant mechanism, which consists of silicon links and polymer (PDMS) soft joints, was produced using a two-dimensional microfabrication process and subsequently folded to obtain a three-dimensional parallel robotic structure. The combination of a compliant parallel mechanism with integrated tweezers and piezoelectric bender actuators leads to a lightweight structure. Because of its low inertia and the closed-loop

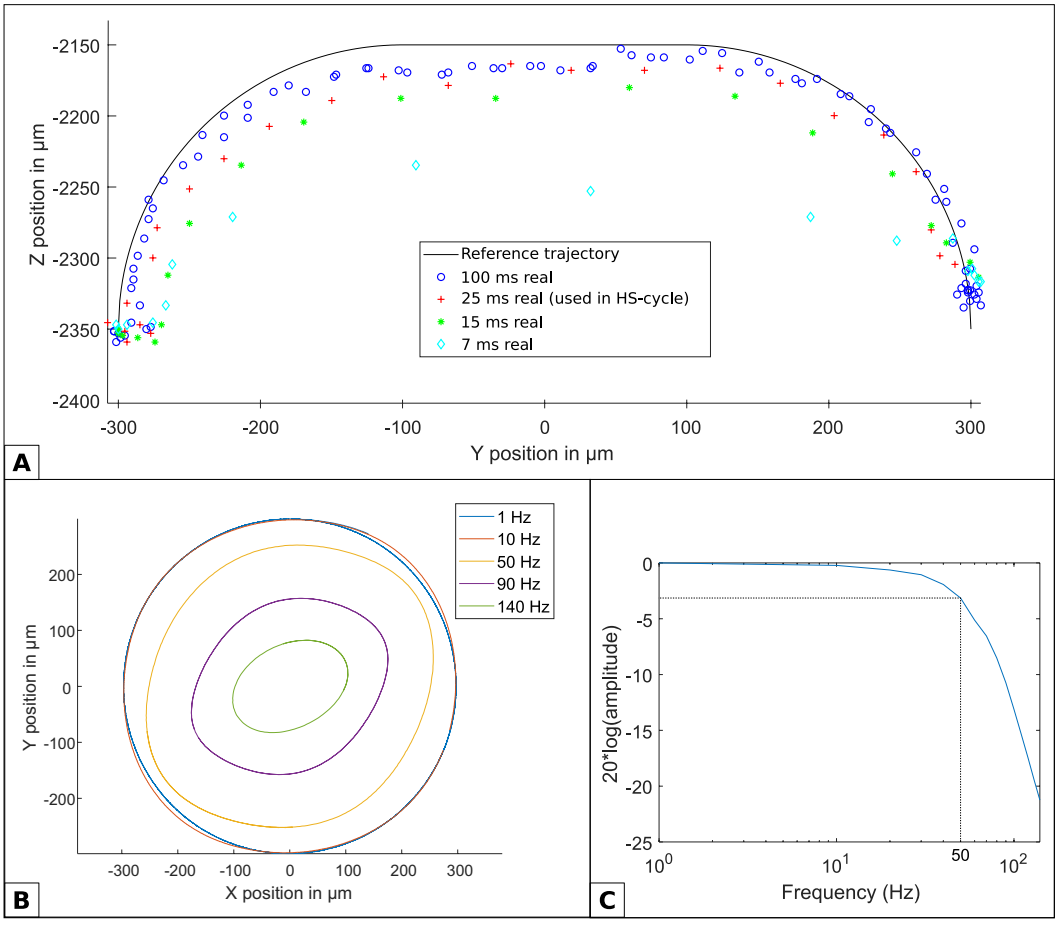

Fig. 6. Experimental high speed trajectories with no load. (**A**) Side view (*OYZ*) of the platform trajectory for the forward trajectory using different traveling times. (**B**) Top view (*OXY*) of the configurable platform trajectory for 600-µm-diameter circular reference trajectory using different cycle times. (**C**) Bode analysis of the amplitude of the trajectories described in (B).

control of its high bandwidth actuators, MiGriBot was able to perform high-speed pick-and-place operations and to reach a precision down to a micrometer.

Most pick-and-place micro/nanomanipulation-cycle durations reported in the scientific literature range from 6 to 48 s (*40*–*43*). Nevertheless, two other works in particular that focused on high-speed pick-and-place operations were able to reach cycle times of 960 ms (*44*) and 800 ms (*45*), both for 60-µm displacements. The equivalent MiGriBot cycle time reported in this work was 80 ms for a 600-µm displacement. This means that MiGriBot is 10 times faster than the fastest pick-and-place micromanipulation system reported so far, with a displacement 10 times larger. Furthermore, because the gripper is part of the robot, we envisage many MiGriBots working in parallel simultaneously and manipulating millions of micro/nano-objects in a microfactory (fig. S7). This type of miniaturized parallel robot with integrated grasping creates an opportunity for high-speed micromanipulation and microassembly operations in manufacturing industries with these characteristics and performances in terms of dimension, precision, and throughput.

The positioning precision of MiGriBot depends on the performance of the actuators and the quality of the mechanical structure. The measured precision of the actuator extension tips is five times better than the robot-positioning precision in *Z* and three times better than the precision of the robot on the *y* axis. This can be explained by the coupling and amplification factor of the parallel architecture, combined with the viscoelasticity effect of the soft joints. Nevertheless, the soft joints allow much larger deformations than hinges in monolithic structures, leading to larger ranges of motion and larger workspaces for comparable structure sizes.

From a design point of view, the performances of the robot described in this study are the result of a trade-off between the size of the robot, its workspace, and its manipulation throughput. The size of current workspace was designed to be relatively comparable with those of large-scale robotic manipulators (the placement of 40-µm objects along 1 mm is comparable with the placement of 40-mm objects along 1 m). To manipulate smaller objects, one can simply reduce the lengths of the actuator's extension, which is one of the main design parameters of the robot. In this case, the robot's workspace would be smaller, but its precision would be higher. Furthermore, because the robot's dynamics are currently limited by the actuator's bandwidth (110 Hz) and not by the first resonance frequency of the compliant structure (264 Hz), such a design choice would also increase the robot's throughput. The cutoff frequency of the actuation system is currently twice as slow as the first resonance frequency of the parallel mechanism. The goal was to obtain the maximum bandwidth allowed by the actuators. Nevertheless, reducing the lengths of the actuators' extensions would decrease their inertia and increase the bandwidth of the actuation system. To prevent any damage to the parallel mechanism, it should be reduced accordingly to also increase its resonance frequency. Thus, manipulating smaller objects in a smaller workspace would be faster and more precise.

Although the proposed robot architecture was designed and tested for microscale pick-and-place operations, it may also be of interest in nanomanipulation. The proposed kinematic architecture has the potential to be miniaturized further. However, the fabrication of such a robotic manipulator at the nanoscale is still a challenge. Although the fabrication of the parallel mechanism is mainly based on fully accurate microfabrication techniques that can produce smaller structures, the parallel mechanisms' assembly onto the actuation system and the tweezers' assembly on the platform are currently

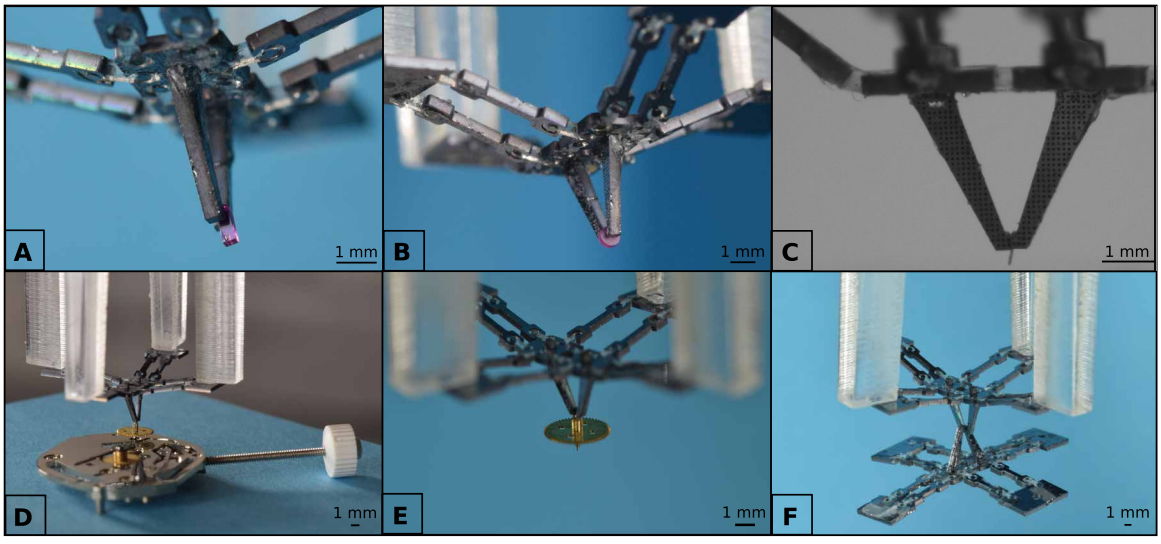

Fig. 7. Manipulation of objects with various shapes and sizes. (**A**) Grasping of a mechanical watch component (lever from a Swiss lever escapement), which is a parallelepiped ruby with a section of 150 μm by 150 μm and a height of 900 μm. (**B**) Manipulation of a cylindrical ruby with a diameter of 700 μm and a thickness of 200 μm. (**C**) Manipulation of a wire with a diameter of 40 μm. (**D**) Extraction of an axis from a watch mechanism; the held diameter is 100 μm. (**E**) Close-up view of the grasped clockwork axis. (**F**) Manipulation of another parallel mechanism constituting our robotic micromanipulator. The width of the grasped component of the micromanipulator was 400 μm.

performed manually. The use of high-precision microassembly robots would probably be necessary to assemble more miniature structures and to reduce the assembly uncertainties (*46*, *47*).

MATERIALS AND METHODS

Experimental setup

The experimental setup used to control and characterize the proposed kinematic structure was composed of four parts: a real-time controller, an actuation controller, vision systems, and a substrate. The real-time control was performed using a dSpace RTI1104 card that runs at 2 kHz and delivers four ±5-V analog signals. The analog signals were then sent to two E-651 drivers that controlled the four piezoelectric multilayer bending actuators (P-871.112 PICMA, distributed by Physik Instrumente GmbH). The feedback control was performed through the integration of the calibrated strain gauges into the actuators to measure their positions.

Two vision systems were used to characterize the robot's performances and observe the pick-and-place operations. The first vision system was composed of two cameras distributed by IDS, UI-3280CPM-GL Rev2 and UI-3040CP-M-GL Rev2, for the side view (*OYZ*) and the bottom view (*OXY*), respectively. The bottom view was obtained via a 45° mirror and a camera whose axis was placed along the *y* axis. This visual setup was used for quasi-static applications and low-speed displacements because these cameras have a standard acquisition frame rate. For the high-speed displacements, we used a second visual system composed of a high-speed camera, Phantom Miro M310, and an external light-emitting diode (LED) lighting. The main challenge was obtaining good image contrast, a large depth of focus, and a low micrometer-to-pixel ratio for the post-treatment of the images.

The last part of the experimental setup was the substrate and the object grasped on it. In most of the experiments, the grasped object was a cylinder with a diameter of 350 μm and a height of 400 μm, made of silicon. Because of the size of the object and the adhesion forces that predominate at this scale, the release of the object could have been problematic. To avoid release issues, a Gel-Pak-4 film was used as a substrate. More details about the experimental setup can be found in the Supplementary Materials, as well as a block diagram (fig. S4) and pictures (fig. S5).

Modeling and design of the robot

The robot and the experimental setup were designed using Solidworks 2018. The computer used for the modeling and the simulation was a PC equipped with an Intel Core i5-10400H CPU running at 2.60 GHz and 16 GB of RAM.

FEA was carried out using Ansys 2019. Because soft joints experience large deformations, a large deformation solver was used, which induced a high computational time. To reduce computational time for the different analyses, the first deformation in the analysis, which was the displacement from the planar initial configuration to the home configuration (Fig. 3), was performed only once. Other simulations were computed from this home-configuration state, which reduced the running time of the simulation. This home configuration was also used as the reference position for the modal analysis of the structure.

The finite element model was used to simulate the forward kinematics of the robot and to carry out the modal analysis. However, to control the robot in real time, the finite element method was too slow. Therefore, we established the inverse kinematics of the robot by solving the closure equations and considering that the joints were perfectly spherical. The soft joints were designed to act as spherical joints.

This design was introduced and validated previously with experiments in (*28*), and comparisons between the finite element model and the kinematic model showed that the position errors did not exceed 5% of the workspace length. During the pick-and-place cycles, the trajectory generation was performed in real time with

trapezoidal speed profiles and using the inverse kinematics of the parallel structure.

Parallel mechanism fabrication

Because the parallel mechanism in this study is composed of PDMS joints and rigid silicon parts, a specific microfabrication process was developed and published in (*28*). PDMS is particularly well suited to the fabrication of micro-soft joints. It is a fluid polymer that can be easily molded in small holes (400 μm in this case). In addition, because after polymerization PDMS is soft, its bending does not require excessively high forces/moments from the actuators. This was required to obtain kinematic behavior close to that of spherical joints.

The first step in the process consisted of a deposition of a 2-μm layer of aluminum on the backside of a silicon wafer, which was used as a stop layer for etching. Second, spin coating of a 7-μm layer of photoresist was performed on the front side. The structures of the manipulator and tweezers were then obtained by the deep reactive-ion etching technique through the silicon wafer. Before molding the PDMS, we performed a spray coating of photoresist on the front side of the wafer to create the specific areas in which the PDMS would be placed. After this step, a wafer support was bonded with vacuum-compatible oil to support the etched wafer and the aluminum membrane. Next, the etched areas were filled with PDMS. Last, the support wafer, the remaining PDMS, and the aluminum membrane were released to obtain the parallel mechanism and the tweezers. To obtain the final manipulator mechanism, two fingers of the tweezers were manually assembled on each part of the configurable platform (Fig. 3A).

After this step, the parallel mechanism was ready to be glued onto the actuators' extensions (Fig. 3B). The key issues at this stage were maintaining the planar configuration during the assembly and the alignment of the silicon links with the actuator's axes. A specific mechanical support was designed and used during the gluing operation to assist in the appropriate positioning of the mechanism. Once the mechanism was attached to the actuators, it had to be moved away from the planar configuration, which was singular, to obtain the home configuration (Fig. 3C). Linear positioning stages were thus used to place the actuators at their reference positions. If the gravity force was not sufficient to displace the parallel mechanism to the right position, a little force along the z axis was applied on the platform to reach the home configuration (Fig. 3D). A known issue when using PDMS with silicon is that both materials do not stick well together. In other words, the adherence between PDMS soft joints and silicon part is low. To ensure the stability of the joints, puzzle shapes were used with a small cylinder inside the tenon to prevent dislocation. Several robots were produced with success and no breakage was noticed, even after high-speed displacements during the experimental campaign, showing that the links were reliable.

SUPPLEMENTARY MATERIALS

www.science.org/doi/10.1126/scirobotics.abn4292
Text
Table S1
Figs. S1 to S7
Movies S1 to S9

REFERENCES AND NOTES

1. H. McClintock, F. Z. Temel, N. Doshi, J.-s. Koh, R. J. Wood, The milliDelta: A high-bandwidth, high-precision, millimeter-scale delta robot. *Sci. Robot.* **3**, eaar3018 (2018).
2. J.-P. Merlet, *Parallel Robots* (Springer Science & Business Media, 2006), vol. 128.
3. R. Clavel, A fast robot with parallel geometry, in *Proceedings of the International Symposium on Industrial Robots* (International Federation of Robotics, 1988), pp. 91–100.
4. F. Pierrot, C. Reynaud, A. Fournier, Delta: A simple and efficient parallel robot. *Robotica* **8**, 105–109 (1990).
5. M. Gauthier, C. Clevy, P. Kallio, D. Heriban, Industrial tools for micromanipulation, in *Micro-and Nanomanipulation Tools* (Wiley, 2015), pp. 369–392.
6. A. Ghosh, B. Corves, *Introduction to Micromechanisms and Microactuators* (Springer, 2015).
7. C. Shi, D. K. Luu, Q. Yang, J. Liu, J. Chen, C. Ru, S. Xie, J. Luo, J. Ge, Y. Sun, Recent advances in nanorobotic manipulation inside scanning electron microscopes. *Microsyst. Nanoeng.* **2**, 16024 (2016).
8. M. Richard, R. Clavel, Concept of modular flexure-based mechanisms for ultra-high precision robot design. *Mech. Sci.* **2**, 99–107 (2011).
9. Y. Bellouard, *Microrobotics: Methods and Applications* (CRC Press, 2019).
10. D. Brouwer, B. de Jong, H. Soemers, Design and modeling of a six DOFs MEMS-based precision manipulator. *Precis. Eng.* **34**, 307–319 (2010).
11. R. Zhang, A. Sherehiy, D. Wei, D. O. Popa, Design and characterization of solid articulated four axes microrobot for microfactory applications. *J. Micro Bio Robot.* **15**, 119–131 (2019).
12. S. H. Yang, Y.-S. Kim, J.-M. Yoo, N. G. Dagalakis, Microelectromechanical systems based stewart platform with sub-nano resolution. *Appl. Phys. Lett.* **101**, 061909 (2012).
13. C. E. Bryson, D. C. Rucker, Toward parallel continuum manipulators, in *Proceedings of the 2014 IEEE International Conference on Robotics and Automation (ICRA)* (IEEE, 2014), pp. 778–785.
14. C. B. Black, J. Till, D. C. Rucker, Parallel continuum robots: Modeling, analysis, and actuation-based force sensing. *IEEE Trans. Robot.* **34**, 29–47 (2017).
15. B. Mauze, R. Dahmouche, G. J. Laurent, A. N. Andre, P. Rougeot, P. Sandoz, C. Clevy, Nanometer precision with a planar parallel continuum robot. *IEEE Robot. Autom. Lett.* **5**, 3806–3813 (2020).
16. F. Largilliere, V. Verona, E. Coevoet, M. Sanz-Lopez, J. Dequidt, C. Duriez, Real-time control of soft-robots using asynchronous finite element modeling, in *Proceedings of the 2015 IEEE International Conference on Robotics and Automation (ICRA)* (IEEE, 2015), pp. 2550–2555.
17. M. Gazzola, L. H. Dudte, A. G. McCormick, L. Mahadevan, Forward and inverse problems in the mechanics of soft filaments. *R. Soc. Open Sci.* **5**, 171628 (2018).
18. J. Till, V. Aloi, C. Rucker, Real-time dynamics of soft and continuum robots based on Cosserat rod models. *Intl. J. Robot. Res.* **38**, 723–746 (2019).
19. B. Mauzé, G. J. Laurent, R. Dahmouche, C. Clévy, Micrometer positioning accuracy with a planar parallel continuum robot. *Front. Robot. AI* **8**, 706070 (2021).
20. J. E. Correa, J. Toombs, N. Toombs, P. M. Ferreira, Laminated micro-machine: Design and fabrication of a flexure-based delta robot. *J. Manufact. Process.* **24**, 370–375 (2016).
21. H. Suzuki, R. J. Wood, Origami-inspired miniature manipulator for teleoperated microsurgery. *Nat. Mach. Intel.* **2**, 437–446 (2020).
22. S. Mintchev, M. Salerno, A. Cherpillod, S. Scaduto, J. Paik, A portable three-degrees- of-freedom force feedback origami robot for human–robot interactions. *Nat. Mach. Intel.* **1**, 584–593 (2019).
23. M. Z. Miskin, A. J. Cortese, K. Dorsey, E. P. Esposito, M. F. Reynolds, Q. Liu, M. Cao, D. A. Muller, P. L. McEuen, I. Cohen, Electronically integrated, mass-manufactured, microscopic robots. *Nature* **584**, 557–561 (2020).
24. D. E. Vogtmann, S. K. Gupta, S. Bergbreiter, Characterization and modeling of elastomeric joints in miniature compliant mechanisms. *J. Mech. Robot.* **5**, 041017 (2013).
25. A. DeMario, J. Zhao, Development and analysis of a three-dimensional printed miniature walking robot with soft joints and links. *J. Mech. Robot.* **10**, 041005 (2018).
26. J. Zhang, Z. Ren, W. Hu, R. H. Soon, I. C. Yasa, Z. Liu, M. Sitti, Voxelated three-dimensional miniature magnetic soft machines via multimaterial heterogeneous assembly. *Sci. Robot.* **6**, eabf0112 (2021).
27. D. Martella, S. Nocentini, D. Nuzhdin, C. Parmeggiani, D. S. Wiersma, Photonic microhand with autonomous action. *Adv. Mater.* **29**, 1704047 (2017).
28. W. Haouas, R. Dahmouche, J. Agnus, N. L. Fort-Piat, G. J. Laurent, New integrated silicon-PDMS process for compliant micro-mechanisms. *J. Micromech. Microeng.* **27**, 127001 (2017).
29. Z. Zhang, X. Wang, J. Liu, C. Dai, Y. Sun, Robotic micromanipulation: Fundamentals and applications. *Annu. Rev. Control. Robot. Autonom. Syst.* **2**, 181–203 (2019).
30. R. Li, H. Qiao, A survey of methods and strategies for high-precision robotic grasping and assembly tasks—Some new trends. *IEEE/ASME Trans. Mechatron.* **24**, 2718–2732 (2019).
31. P. Lambert, J. L. Herder, Parallel robots with configurable platforms: Fundamental aspects of a new class of robotic architectures. *Proc. Inst. Mech. Eng. C J. Mech. Eng. Sci.* **230**, 463–472 (2016).
32. P. Lambert, J. L. Herder, A 7-DOF redundantly actuated parallel haptic device combining 6-DOF manipulation and 1-DOF grasping. *Mech. Mach. Theory* **134**, 349–364 (2019).

33. F. Pierrot, O. Company, H4: A new family of 4-DOF parallel robots, in *Proceedings of the 1999 IEEE/ASME International Conference on Advanced Intelligent Mechatronics (Cat. No.99TH8399)* (IEEE, 1999), pp. 508–513.
34. F. Pierrot, O. Company, F. Marquet, A new high-speed 4-DOF parallel robot synthesis and modeling issues. *IEEE Trans. Robot. Autom.* **19**, 411–420 (2003).
35. B.-J. Yi, H. Y. Na, J. H. Lee, Y. S. Hong, S. R. Oh, I. H. Suh, W. K. Kim, Design of a parallel-type gripper mechanism. *Intl. J. Robot. Res.* **21**, 661–676 (2002).
36. V. Babin, C. Gosselin, Mechanisms for robotic grasping and manipulation. *Annu. Rev. Control. Robot. Autonom. Syst.* **4**, 573–593 (2021).
37. W. Haouas, R. Dahmouche, N. Le Fort-Piat, G. J. Laurent, A new seven degrees-of-freedom parallel robot with a foldable platform. *J. Mech. Robot.* **10**, 045001 (2018).
38. F. Pierrot, V. Nabat, O. Company, S. Krut, P. Poignet, Optimal design of a 4-DOF parallel manipulator: From academia to industry. *IEEE Trans. Robot.* **25**, 213–224 (2009).
39. R. N. Jazar, *Theory of Applied Robotics, Kinematics, Dynamics and Control* (Springer, ed. 2, 2010).
40. Y. Zhang, B. K. Chen, X. Liu, Y. Sun, Autonomous robotic pick-and-place of microobjects. *IEEE Trans. Robot.* **26**, 200–207 (2009).
41. R. K. Jain, S. Majumder, B. Ghosh, S. Saha, Design and manufacturing of mobile micro manipulation system with a compliant piezoelectric actuator based micro gripper. *J. Manufact. Syst.* **35**, 76–91 (2015).
42. M. Lofroth, E. Avci, Development of a novel modular compliant gripper for manipulation of micro objects. *Micromachines* **10**, 313 (2019).
43. H. Xie, S. Régnier, Three-dimensional automated micromanipulation using a nanotip gripper with multi-feedback. *J. Micromech. Microeng.* **19**, 075009 (2009).
44. E. Avci, K. Ohara, C. N. Nguyen, C. Theeravithayangkura, M. Kojima, T. Tanikawa, T. Arai, High-speed automated manipulation of microobjects using a two-fingered microhand. *IEEE Trans. Indust. Electron.* **62**, 1070–1079 (2014).
45. E. Kim, M. Kojima, Y. Mae, T. Arai, High-speed manipulation of microobjects using an automated two-fingered microhand for 3D microassembly. *Micromachines* **11**, 534 (2020).
46. A. Benouhiba, L. Wurtz, J.-Y. Rauch, J. Agnus, K. Rabenorosoa, C. Clevy, NanoRobotic structures with embedded actuation via ion induced folding. *Adv. Mater.* **33**, 2103371 (2021).
47. J.-Y. Rauch, O. Lehmann, P. Rougeot, J. Abadie, J. Agnus, M. A. Suarez, Smallest microhouse in the world, assembled on the facet of an optical fiber by origami and welded in the μRobotex nanofactory. *J. Vacuum Sci. Technol. A Am. Vacuum Soc.* **36**, 041601 (2018).

Acknowledgments: We thank J. Agnus and D. Belharet for technological assistance during the clean-room fabrication. **Funding:** This work was supported by the Grand Besançon Métropole, the French ANR project MiniSoRo (ANR-19-CE10-0004), the ROBOTEX network (ANR-21-ESRE-0015), and the EUR EIPHI program (ANR-17-EURE-0002). This work was carried out in part within the French RENATECH network and its FEMTO-ST technological facility.
Author contributions: R.D. proposed the original idea and the robot architecture. W.H., G.J.L., and R.D. initiated the project. M.L. and W.H. fabricated the robot. M.L. performed the numerical simulations and the experimental tests, managed the statistical analysis of the data, and wrote the first draft of the paper. G.J.L. and W.H. assisted M.L. with the modeling. All authors contributed to the methodology and to the manuscript preparation. M.L., G.J.L., and M.G. contributed to the data presentation and visualization. G.J.L., M.G., and R.D. managed the research project, including the provision of resources and funding acquisition. **Competing interests:** The authors declare that they have no competing interests. **Data and materials availability:** All data needed to support the conclusions of this manuscript are included in the main text or Supplementary Materials. The FEA data are available on Zenodo https://doi.org/10.5281/zenodo.6910861

Submitted 30 November 2021
Accepted 27 July 2022
Published 24 August 2022
10.1126/scirobotics.abn4292

Science Robotics

MiGriBot: A miniature parallel robot with integrated gripping for high-throughput micromanipulation

Maxence Leveziel, Wissem Haouas, Guillaume J. Laurent, Michaël Gauthier, and Redwan Dahmouche

Sci. Robot. **7** (69), eabn4292. DOI: 10.1126/scirobotics.abn4292

Science Robotics (ISSN 2470-9476) is published by the American Association for the Advancement of Science. 1200 New York Avenue NW, Washington, DC 20005. The title *Science Robotics* is a registered trademark of AAAS.